AD-A008 345

STUDY OF REACTION MECHANISM IN TRACER MUNITIONS

Alexander P. Hardt, et al

Lockheed Missiles and Space Company, Incorporated

Prepared for:

Frankford Arsenal

December 1974

UNCLASSIFIED

SECURITY CLASSIFICATION OF THIS PAGE (When Data Entered)

REPORT DOCUMENTATION PAGE

READ INSTRUCTIONS BEFORE COMPLETING FORM

1. REPORT NUMBER: FA-TR-74047	2. GOVT ACCESSION NO.
3. RECIPIENT'S CATALOG NUMBER: AD-A008 345	
4. TITLE (and Subtitle): STUDY OF REACTION MECHANISM IN TRACER MUNITIONS	5. TYPE OF REPORT & PERIOD COVERED: Technical Research Report
	6. PERFORMING ORG. REPORT NUMBER
7. AUTHOR(s): Alexander P. Hardt and Peter V. Phung (Lockheed Missiles & Space Company, Inc.) Thomas Doris - Coordinator	8. CONTRACT OR GRANT NUMBER(s): DAAA25-73-C-0675
9. PERFORMING ORGANIZATION NAME AND ADDRESS: Lockheed Missiles & Space Company, Inc. Lockheed Palo Alto Research Laboratory 3251 Hanover Street, Palo Alto, CA 94304	10. PROGRAM ELEMENT, PROJECT, TASK AREA & WORK UNIT NUMBERS
11. CONTROLLING OFFICE NAME AND ADDRESS: Frankford Arsenal Attn: SARFA-MDP-Y Philadelphia, PA 19137	12. REPORT DATE: December 1974
	13. NUMBER OF PAGES: 56 57
14. MONITORING AGENCY NAME & ADDRESS(if different from Controlling Office)	15. SECURITY CLASS. (of this report): Unclassified
	15a. DECLASSIFICATION/DOWNGRADING SCHEDULE: N/A

16. DISTRIBUTION STATEMENT (of this Report)

Approved for public release; distribution unlimited.

17. DISTRIBUTION STATEMENT (of the abstract entered in Block 20, if different from Report)

18. SUPPLEMENTARY NOTES

19. KEY WORDS (Continue on reverse side if necessary and identify by block number)

Tracer Munitions
Tracer Reactions
Thermal Analysis
Thermal Conductivities
Nitrate Kinetics
Equilibrium Calculations
Burning Rates

20. ABSTRACT (Continue on reverse side if necessary and identify by block number)

A study of reaction mechanisms in tracer munitions was performed in which the attempt was made to assess the parametric importance of the mixture characteristics in determining the burning rate and, to the extent possible, on trace duration and visibility. Kinetic data on the decomposition of strontium nitrate and of polyvinyl chloride were measured, as were the thermal conductivities of several tracer mixtures of varying fuel-to-oxidizer ratios. Heat transfer into the solid tracer mixture was

DD FORM 1 JAN 73 1473 EDITION OF 1 NOV 65 IS OBSOLETE

UNCLASSIFIED

SECURITY CLASSIFICATION OF THIS PAGE (When Data Entered)

20. ABSTRACT - (cont'd)

analyzed numerically, and the heat flux was obtained from experimentally determined burning rates of stationary and spinning tracer bullets. The presence of the binder was neglected in the analytical study.

By assuming that the metal oxide was generated in the gas phase, the thickness of the reaction zone was obtained as a function of the particle size. Burning rates were computed as a function of heat flux for various fuel-to-oxidizer ratios. The application of these findings to tracer munitions still requires experimentally determined burning rates that define the partition between the heat flux into the solid and the total heat generated by the tracer reaction.

The understanding of tracer reactions which was achieved in this study will be valuable in other applications of metal-oxidant systems such as flares and fumer bullets.

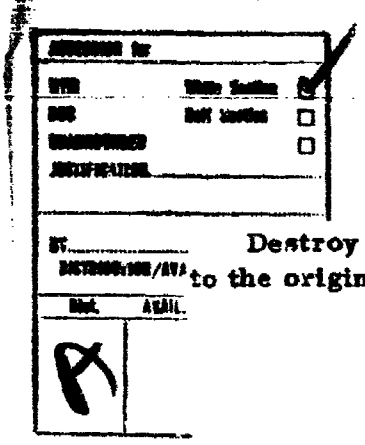

DISPOSITION INSTRUCTIONS

Destroy this report when it is no longer needed. Do not return it to the originator.

The findings in this report are not to be construed as an official Department of the Army position unless so designated by other authorized documents.

CONTENTS

Section		Page
	NOMENCLATURE	5
1	INTRODUCTION	6
	1.1 Description of Gasforming Pyrotechnic Reaction	6
	1.2 Description of Tracer Reaction	7
	1.3 Objective	10
	1.4 Technical Approach	10
2	EXPERIMENTAL STUDY	12
	2.1 Decomposition Kinetics of Strontium Nitrate	12
	2.1.1 Literature Survey	12
	2.1.2 Experimental Study	13
	2.2 Particle Size Distribution of Magnesium	15
	2.3 Thermal Degradation of Polyvinyl Chloride	17
	2.4 Equilibrium Calculations for Various Tracer Compositions	22
	2.5 Thermal Transport Properties of Tracer Mixtures	30
3	ANALYTICAL STUDY	32
	3.1 Solid-Phase Process	32
	3.2 Gas-Phase Reaction	35
	3.2.1 Introduction	35
	3.2.2 Determination of the Magnesium Droplet Lifetime	36
	3.2.3 Calculation of Reaction Zone Thickness	37
4	RESULTS	40

Section		Page
5	RECOMMENDATIONS	45
6	SUMMARY AND CONCLUSIONS	46
7	REFERENCES	47
Appendix		
A	COMPUTER PROGRAM FOR THERMAL TRANSPORT IN THE SOLID	48
B	CALCULATION OF ENERGY PARTITION	53
DISTRIBUTION		54

ILLUSTRATIONS

Figure		Page
1	Models for Burning of Magnesium Particle	9
2	Decomposition Rate Data for Strontium Nitrate	14
3	Reaction Rate Constants for the Reaction $2\ Sr(NO_3)_2 \rightarrow 2\ SrO + 4\ NO + 3\ O_2$	16
4	Magnesium Powder 100×	16
5	Fraction of HCl Remaining in Polyvinyl Chloride at 252°C as a Function of Time	18
6	Thermal Degradation of Polyvinyl Chloride Test of 3/2 Order Reaction Rate Law	20
7	Thermal Decomposition of Polyvinyl Chloride – Plot of Reaction Rate Constants	21
8	Thermal Conductivity of $Mg\text{-}Sr(NO_3)_2$ Mixtures	31
9	Effect of Fuel Particle Size on Reaction Zone Thickness	39
10	Temperature Distribution in Solid	41
11	Computed Reaction Rates as Function of Heat Flux	42

TABLES

Table		Page
1	Results of I east Square Analysis of Strontium Nitrate Decomposition Rate Data	15
2	Rate Constants for the Thermal Degradation of Polyvinyl Chloride	19
3	Product Description for Various Tracer Mixtures	23
4	Equilibrium Composition of Reaction Products Tracer Composition (PVC - Mg - Sr $(NO_3)_2$) 28.0 - 9.1 - 63.0 wt %	24
5	Equilibrium Composition of Reaction Products Tracer Composition (PVC - Mg - Sr $(NO_3)_2$) 19.8 - 12.7 - 67.5 wt %	25
6	Equilibrium Composition of Reaction Products Tracer Composition (PVC - Mg - Sr $(NO_3)_2$) 30.0 - 19.4 - 50 wt %	26
7	Equilibrium Composition of Reaction Products Tracer Composition (PVC - Mg - Sr $(NO_2)_3$) 22.1 - 28.5 - 49.6 wt %	27
8	Equilibrium Composition of Reaction Products Tracer Composition (PVC - Mg - Sr $(NO_3)_2$) 17 - 28 - 55 wt %	28
9	Equilibrium Composition of Reaction Products Tracer Composition (PVC - Mg - Sr $(NO_3)_2$) 17 - 33 - 50 wt %	29
10	Thermal Transport Properties of Tracer Mixtures	30
11	Summary of Thermal Processes	33
12	Experimentally Determined Regression Rates (Furnished by Frankford Arsenal)	35
13	Calculated Heat Fluxes and Energy Partitions	43

NOMENCLATURE

B	=	preexponential factor (sec^{-1})
C	=	concentration (g/g)
C_p	=	heat capacity (cal/g°K)
D	=	diffusion coefficient (cm^2/sec)
E	=	activation energy (cal/mole)
F	=	fraction unreacted
H	=	heat flux (cal/cm^2 sec)
k_T	=	reaction rate constant (min^{-1})
M	=	molecular weight (g/mole)
m	=	mass of fuel particle (moles)
P	=	pressure (atm)
Q	=	heat of dissociation (cal/g)
R	=	gas constant (cal/mole °K)
r	=	radius of fuel droplet (cm)
s or x	=	distance increments in solid phase (cm)
T_s	=	surface temperature of solid (°K)
T_a	=	average temperature in the reaction zone (°K)
t	=	time (sec)
t_b	=	evaporation time for droplet (sec)
v	=	regression or burning rate (cm/sec)
w	=	mass flowrate (g/cm^2 sec)
y_n	=	mole fraction of oxidizer in the vapor phase
Z	=	pre exponential factor (min^{-1})
ρ	=	density of fuel (g/cm^3)
ρ_g	=	density of gas phase (g/cm^3)
Ω	=	spin rate of projectile (rpm)
κ	=	thermal conductivity (cal/cm sec °K)

Section 1
INTRODUCTION

1.1 DESCRIPTION OF GASFORMING PYROTECHNIC REACTIONS

During the burn of a pyrotechnic composition, the solid is transformed into a gas by pyrolysis, chemical reaction and evaporation. Even if the transformation occurs through the formation of an intermediate liquid phase, there exists a certain position, called the burning surface, where the gas is being formed. The mechanism of the solid-phase decomposition at the burning surface is considered to be the rate-controlling step, the gas being formed at the rate

$$\rho r = \rho B \exp(-E/RT_s) \tag{1}$$

where

- r = burning rate (cm/sec)
- B = the pre-exponential frequency factor
- E = the activation energy
- R = the gas constant
- T_s = the temperature at the burning surface
- ρ = the density (gm/cm^3)

Reactions occurring in the solid phase would have changed the temperature at the burning surface to T_s', but actually a temperature T_s greater than T_s' is obtained there because heat is conducted back to the solid from the gas. The essential theoretical problem is to discover how T_s depends on the gas-phase process.

Tracer mixtures constitute not homogeneous materials but rather composites that contain both discrete fuel and oxidizer particles, the decomposition of which is governed by Eq. (1). For the steady-state burning of a composite, it is reasonable to assume that the linear rates of regression of the oxidizer and the fuel surfaces are about equal:

$$\rho_f r_f = \rho_o r_o$$

$$\rho_f B_f \exp(-E_s/RT_{sf}) \simeq \rho_f B_o \exp(-E_o/RT_{so}) \qquad (2)$$

where the subscripts f and o refer to the fuel and oxidizer, respectively.

In general, the preexponential factor and the activation energy of the fuel and oxidizer are not equal. It follows that T_{sf} and T_{so} must also differ. Because of the difference in pyrolysis rates, one constituent gasifies relatively faster, and the slower burning component is left protruding from the surface. The faster pyrolysing constituent is therefore in contact with a cooler region of the flame than is the slower burning constituent. Eventually, particles of the slower burning constituent may be ejected entirely from the surface and be entrained in the hot gas stream where they will undergo further reaction.

1.2 DESCRIPTION OF TRACER REACTION

Tracer reactions are well described by the above model. A recent study (Ref. 1) of a motion-picture record of a burning tracer composition has shown that most fuel particles (atomized magnesium) are ejected as molten globules from the surface. Because of the high gas temperature, the fuel particles vaporize so as to give rise by subsequent

oxidation to a hot reaction zone. This flame front is narrow because of the high rate of the gas-phase reaction as compared with the preceding solid-phase decomposition and evaporation steps. The temperature and the proximity of the flame to the surface depends (at constant ambient pressure) on the particle size and the stoichiometry. Tracer compositions are usually fuel-rich, resulting (as will be shown in a later section) in an equilibrium gas composition containing large quantities of magnesium vapor. This combustible gas is largely responsible for the luminous plume of the tracer bullet.

In describing the burning of magnesium particles, two reaction models have been considered (Ref. 2), which differ mainly in the treatment of the condensed oxide formed. Experimental evidence shows that some magnesium particles will react with an oxidizer that surrounds them with a crust of oxide. The reaction rate is determined by the diffusion through this crust which, owing to the higher density of the oxide relative to the parent metal, is porous and readily permits the counterdiffusion of gaseous oxidizer and fuel. The end product is an empty bubble that is usually a part of a cake which which was formed in situ by the interaction with the oxide growth from the neighboring particles. These oxide bubbles are shown in Fig. 1a.

Most of the magnesium becomes entrained in the stream of gaseous oxidizer. While the rate of heat input in the flame zone suffices to cause the magnesium to evaporate, the resulting vapor oxidizes only partially, because of the fuel rich nature of the mixture, so that the oxide particles remain detached from the metal surface. These oxide particles have colloidal dimensions and are entrained in the gas stream with the other products of the reaction. The reaction rate is controlled by the vapor phase diffusion of magnesium to the reaction site. This reaction model best describes the process which we have observed and is illustrated in Fig. 1b.

The theoretical problem in describing tracer reactions is to learn the effects of the stoichiometry and particle size on the rate of energy release in the flame and hence the energy partition between the heat deposited into the solid and the heat entrained in the exhaust gas. The effect of reducing the fuel particle size (at constant composition)

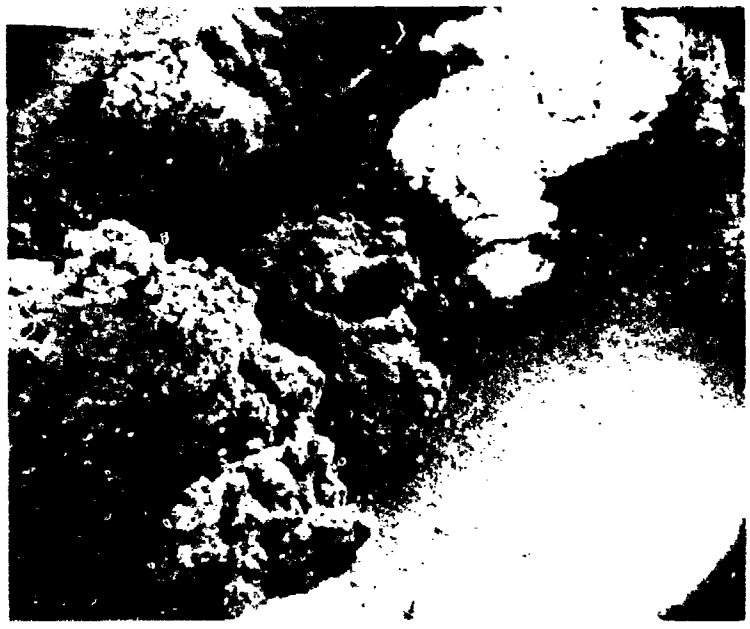

120 μ ⊢——⊣ 85×

Fig. 1a Residual Magnesium Oxide Bubbles. The product was obtained by burning a tracer bullet in an argon-filled chamber and by separating the granular solids from the colloidal dust which adhered to the reactor walls. These hollow bubblee remain after the magnesium particles are coated with an oxide crust followed by flash evaporation of the metal through a vent hole. The rate of this process is too slow to account for the tracer reaction.

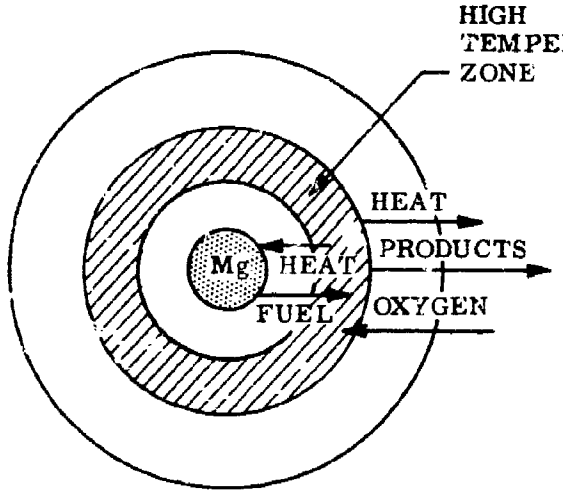

Fig. 1b Predominant Burning Mechanism of Magnesium Particles (Ref. 2)

Fig. 1 Models for Burning of Magnesium Particle

will be to narrow the flame zone and to increase the energy partition and hence the regression rate of the surface. The result will be a brighter plume of shorter duration. Reduction of the fuel (at constant particle size) may reduce thermal conductance in the solid, reduce the regression rate, and prolong but dim the trace. At the extremes in composition, the trace quality will become insensitive to fuel characteristics.

1.3 OBJECTIVE

The purpose of this study is to construct an analytical model that will put the preceding qualititative description on a quantitative basis. An understanding of all the factors that determine the energy partition is beyond the state of the art, and for this reason the baseline conditions were to be determined by experimentally determined regression rates. Inasmuch as this study is of preliminary but otherwise perfectly general, nature, the effect of binders and of color intensifiers on tracer performance has been omitted from the theoretical analysis. However, methods by which such variables can be accounted for and the effect of such additives on the equilibrium composition of the product grades will be described in this report.

1.4 TECHNICAL APPROACH

The rate constants of the decomposition of the components were determined experimentally. The thermochemical properties were collected from published sources. The energy partitions were calculated from several compositions of a single particle size of the magnesium using experimentally determined burning rates of spinning 7.62-mm tracer bullets. Thermal conductivities were measured using the thermal diffusion method (Ref. 3).

The analytical problem concerns the heat transfer into the endothermally decomposing solid with moving boundaries. The gas-phase process was treated by examining the experimental evidence for the case of fuel vapor diffusing through an oxide shell and for the case of a detached reaction zone surrounding the droplets. It was found that only the detached reaction zone model (Fig. 1b) could account for the experimentally observed reaction rates.

Section 2
EXPERIMENTAL STUDY

2.1 DECOMPOSITION KINETICS OF STRONTIUM NITRATE

2.1.1 Literature Survey

The kinetics of the decomposition of inorganic nitrates has never been studied exhaustively, particularly with respect to the alkaline earths, and recent studies are almost completely lacking. This situation is surprising in view of the wide range of applications of inorganic nitrates in the pyrotechnics and fertilizer industry.

The question that had to be answered in this study was whether the nitrate or the nitrite was the more stable, i.e., whether the decomposition of the nitrate could be treated as a first-order reaction with respect to its decomposition or whether some other decomposition step was rate determining. Although no rate data have ever been published, the equilibria have been studied by Centnerzwer (Ref. 4), who found that the nitrite decomposes slowly below its melting point of 264°C:

$$Sr(NO_2)_2 \underset{1\ atm}{\overset{380°C}{\rightleftharpoons}} SrO + N_2O_3 \qquad (3)$$

The nitrous anhydride disproportionates in a fast step:

$$N_2O_3 \rightleftharpoons NO_2 + NO \qquad (4)$$

so that the resulting dioxide can react with more nitrite in another fast reaction:

$$Sr(NO_2)_2 + 2\ NO_2 \rightleftharpoons Sr(NO_3)_2 + 2\ NO \qquad (5)$$

Because the rate of oxidation of the nitrite is greater than the rate of its dissociation, the nitrate will be the more stable specie. This was shown (Ref. 5) by the stability of the nitrate up to 580°C. This stability of the nitrate was confirmed by differential thermal analysis (6). Findings that the nitrate decomposes in several steps starting at 280°C (7) must have been due to test samples that were contaminated by the nitrite.

Alkali nitrates, by contrast, form an intermediate nitrite on decomposition (Ref. 6) which was explained by the fact that alkali nitrates disscciate above the melting point and hence have two degrees of freedom, whereas the alkaline earth nitrates dissociate below the melting point ($Sr(NO_3)_2$, 618°C, Ref. 6) and therefore have only one degree of freedom (Ref. 7).

We conclude from this study that strontium nitrate is stable with respect to its decomposition into the nitrite and that the decomposition is most likely a first order reaction with respect to the nitrate:

$$2\ Sr(NO_3)_2 \longrightarrow 2\ SrO + 4\ NO + 3\ O_2 \qquad (6)$$

2.1.2 Experimental Study

Strontium nitrate was decomposed isothermally in a thermal gravimetric analyzer (TGA). It was found that unless air (containing CO_2) was excluded, the oxide product was converted into the carbonate. Experimental data became reproducible when the decomposition was performed in helium. The resulting weight losses equivalent to $Sr(NO_3)_2$ were used to compute the ratio $\frac{a}{a-x}$ where a was the original weight of the nitrate at time zero, and x was the weight loss. Figure 2 shows these normalized weight loss data plotted as function of time for five temperatures, the slope of the line being the first-order rate constant k_T. The data were treated by a Tymshare least squares routine. The results are shown in Table 1.

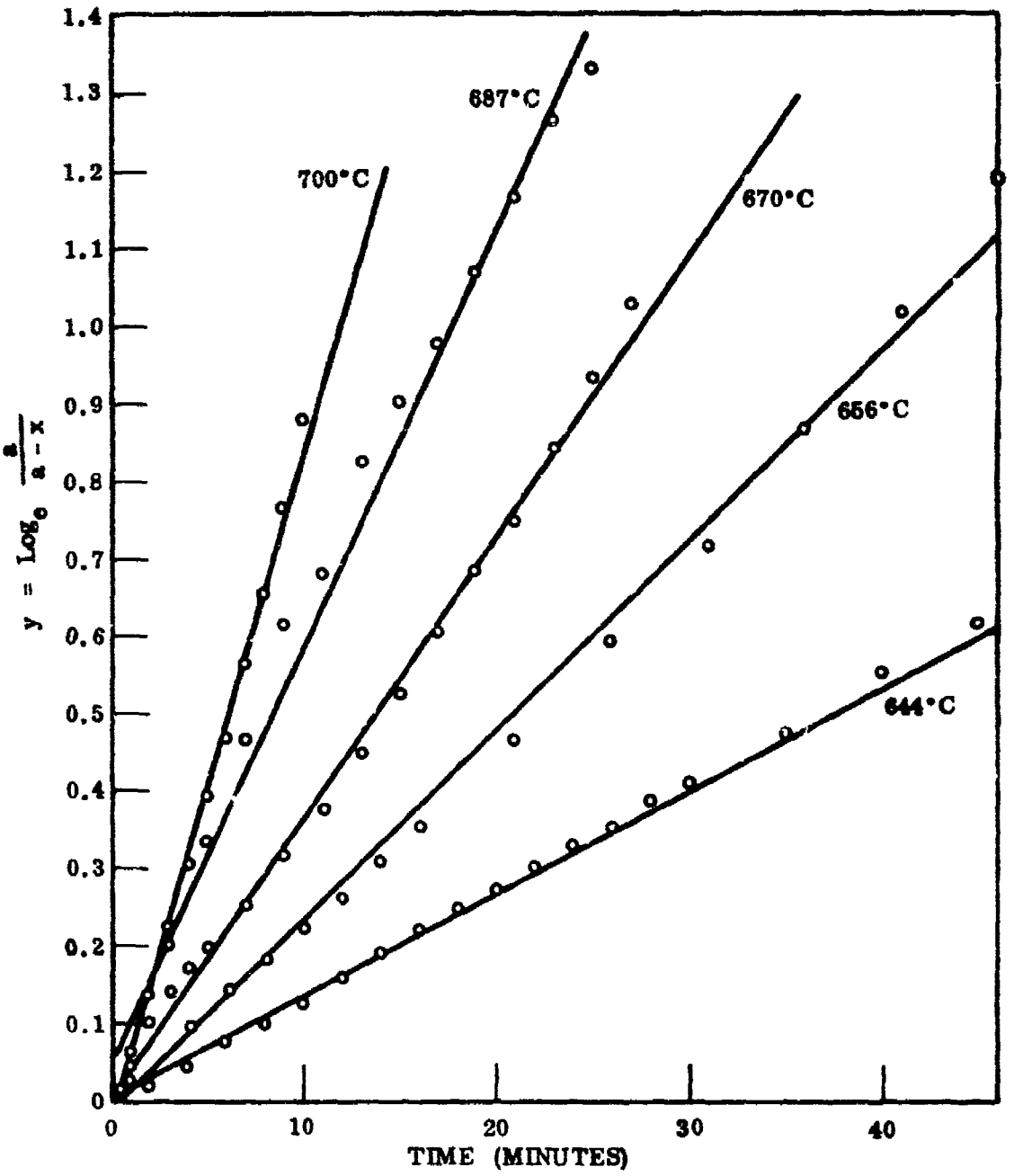

Fig. 2 Decomposition Rate Data for Strontium Nitrate

Table 1

RESULTS OF LEAST SQUARE ANALYSIS OF STRONTIUM NITRATE DECOMPOSITION RATE DATA

Temperature (°K)	Computed $\ln \frac{a}{a-x} = k_T t$	k_T (min^{-1})	Std. Dev. in $\ln \frac{a}{a-x}$
917	0.00470 + 0.01316 t	0.0132	0.0151
929	- 0.01885 + 0.02476 t	0.0248	0.0276
943	0.00582 + 0.03613 t	0.0361	0.0221
960	0.05458 + 0.05363 t	0.0536	0.0454
973	- 0.02179 + 0.08559 t	0.0856	0.0216

The rate constants k_T were correlated with the reciprocal temperature as shown in Fig. 3. The slope of the line is proportional to the energy of activation, E. We conclude that the linear dependence of the decomposition data on time justifies the assumption of a first-order rate law which is expressed as follows:

$$C = C_o e^{-kt} \tag{7}$$

and

$$k_T = Ze^{-\frac{E}{RT}} \tag{8}$$

From Fig. 2

$$E = 55{,}400 \pm 6000 \text{ cal/mole} \quad \text{and} \quad Z = 1 \times 10^{11} \text{ min}^{-1}$$

2.2 PARTICLE SIZE DISTRIBUTION OF MAGNESIUM

Figure 4 shows a scanning electron micrograph of the Frankford Arsenal magnesium. The size distribution was determined by particle count, and the characteristic size was found to be 120 μ.

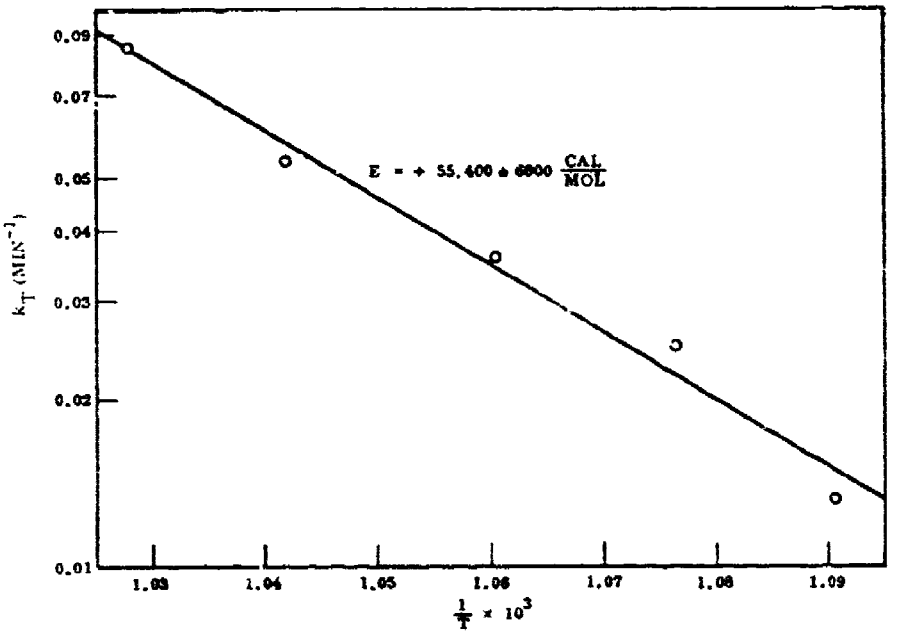

Fig. 3 Reaction Rate Constants for the Reaction 2 $Sr(NO_3)_2$ → 2 SrO + 4 NO + 3 O_2

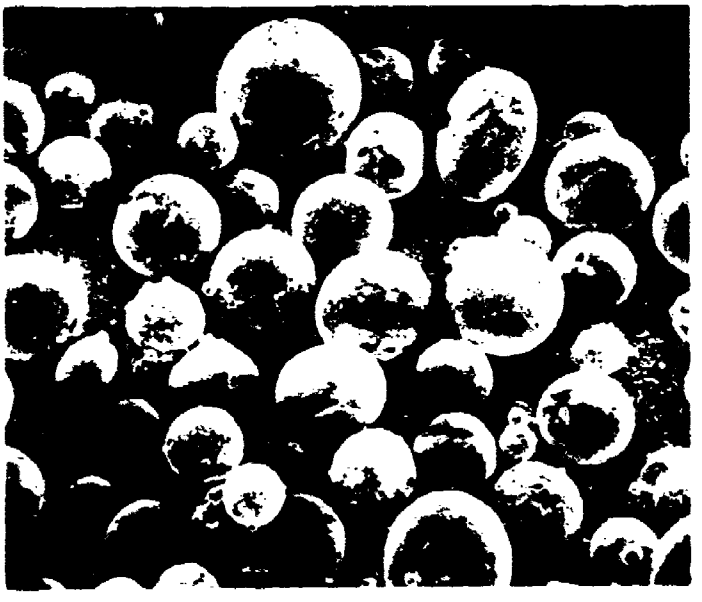

120 μ

Fig. 4 Magnesium Powder 100×

2.3 THERMAL DEGRADATION OF POLYVINYL CHLORIDE

Unlike the dissociation of strontium nitrate, the thermal response of PVC is complex. Figure 5 shows the typical appearance of low-temperature isothermal TGA data. The sigmoid shape of the curve is typical of chain reactions, which for PVC may be visualized as follows. The carbon-chlorine bond is the weakest bond in the polymer so that it is first to rupture. This is followed immediately by an abstraction of a hydrogen atom from an adjacent carbon and the formation of a double bond in the chain.

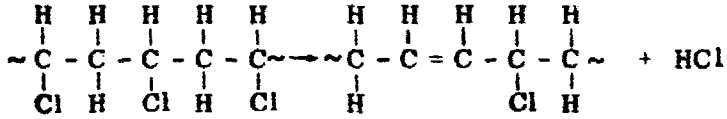

(9)

The chlorine atoms in the β position to the double bond are now more likely to break away from the carbon atoms to which they are attached than the other chlorine atoms. Hence, once one chlorine is removed (requiring a relatively high activation energy, and consequently, a lengthy induction period), the others come off easily, leaving behind a polyunsaturated structure which is prone to further reaction. It may crosslink, rupture, or form cyclic compounds. This explains why the analysis of the volatile decomposition products show in addition to HCl also ethylene, propylene and benzene (Ref. 8). The remainder is a polyacetylene char which is subject to further attack by oxidizers.

The above steps (except for the initial activation) are strongly exothermic, and it has been found that when PVC is heated in a confined volume, it will decompose explosively (Ref. 10). Using differential scanning calorimetry, a value of -72 ±10 cal/g

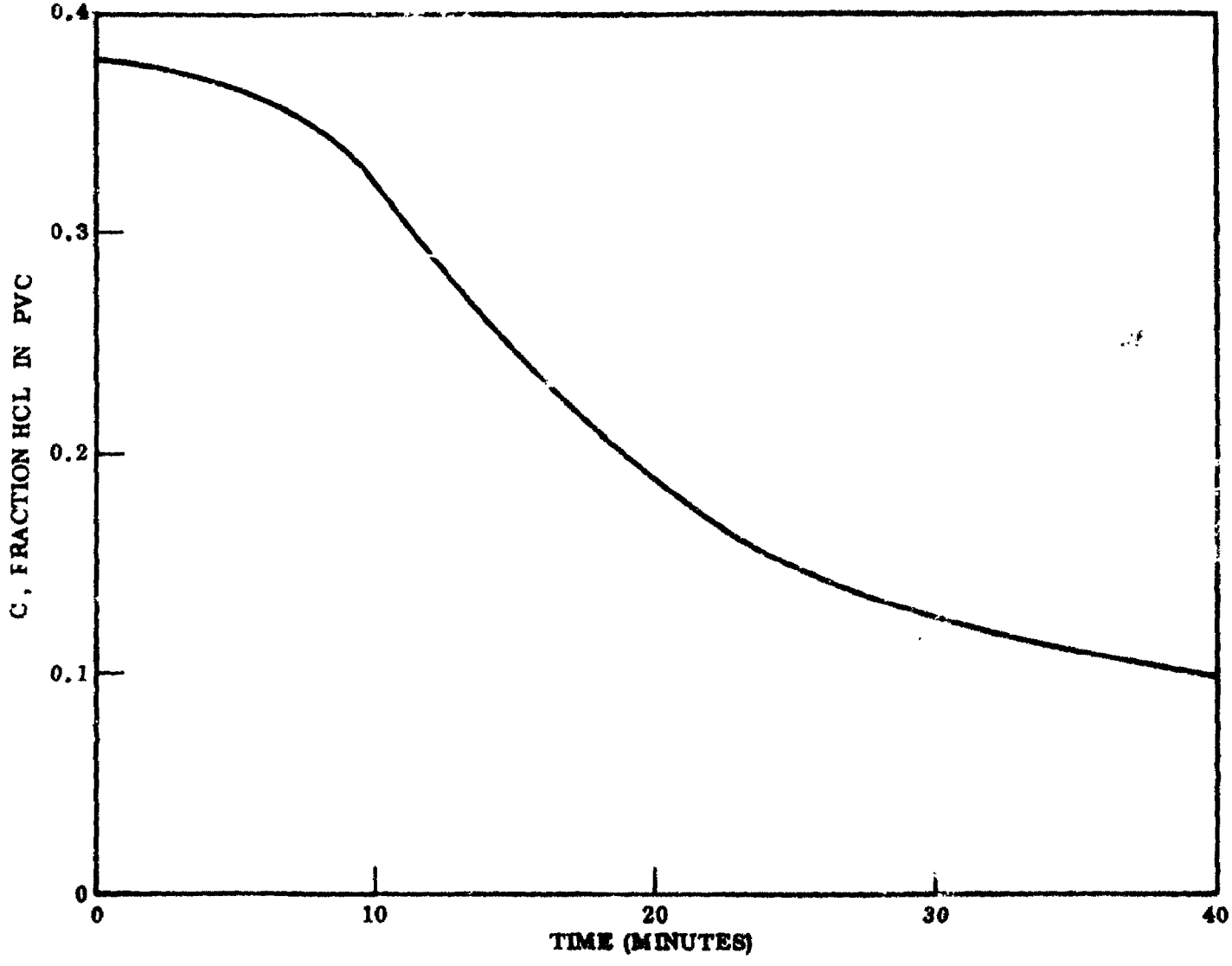

Fig. 5 Fraction of HCl Remaining in Polyvinyl Chloride at 252°C as a Function of Time

was found for the heat of decomposition of PVC. This value is small compared with other thermal quantities that control the reaction. It has therefore been ignored in this study.

Dehydrochlorination of PVC appears to follow a 3/2 order reaction rate law (Ref. 9). The equation for such a reaction is

$$-\frac{dC}{dt} = k\, C^{3/2}$$

which, upon integration, yields

$$C^{-\frac{1}{2}} = C_o^{-\frac{1}{2}} + \frac{1}{2}\, k_T t \qquad (10)$$

where C is the fraction of HCl remaining in the sample at time t, and k_T is the specific reaction rate constant. The fit of the experimental data as obtained from isothermal TGA runs is shown in Fig. 6. An Arrhenius plot based on the resulting rate constants (see Fig. 7) yielded an activation energy of 10,750 cal/mole and a pre-exponential factor of 10^8 min^{-1}, using Eq. (8).

Table 2

RATE CONSTANTS FOR THE THERMAL DEGRADATION OF POLYVINYL CHLORIDE

Temperature (°C)	k_T $C^{-1/2}$/min
252	0.11
272	0.14
294	0.21

We conclude that the presence of PVC in the tracer mixture will complicate the construction of a tracer reaction model in that the presence of two decomposing solids

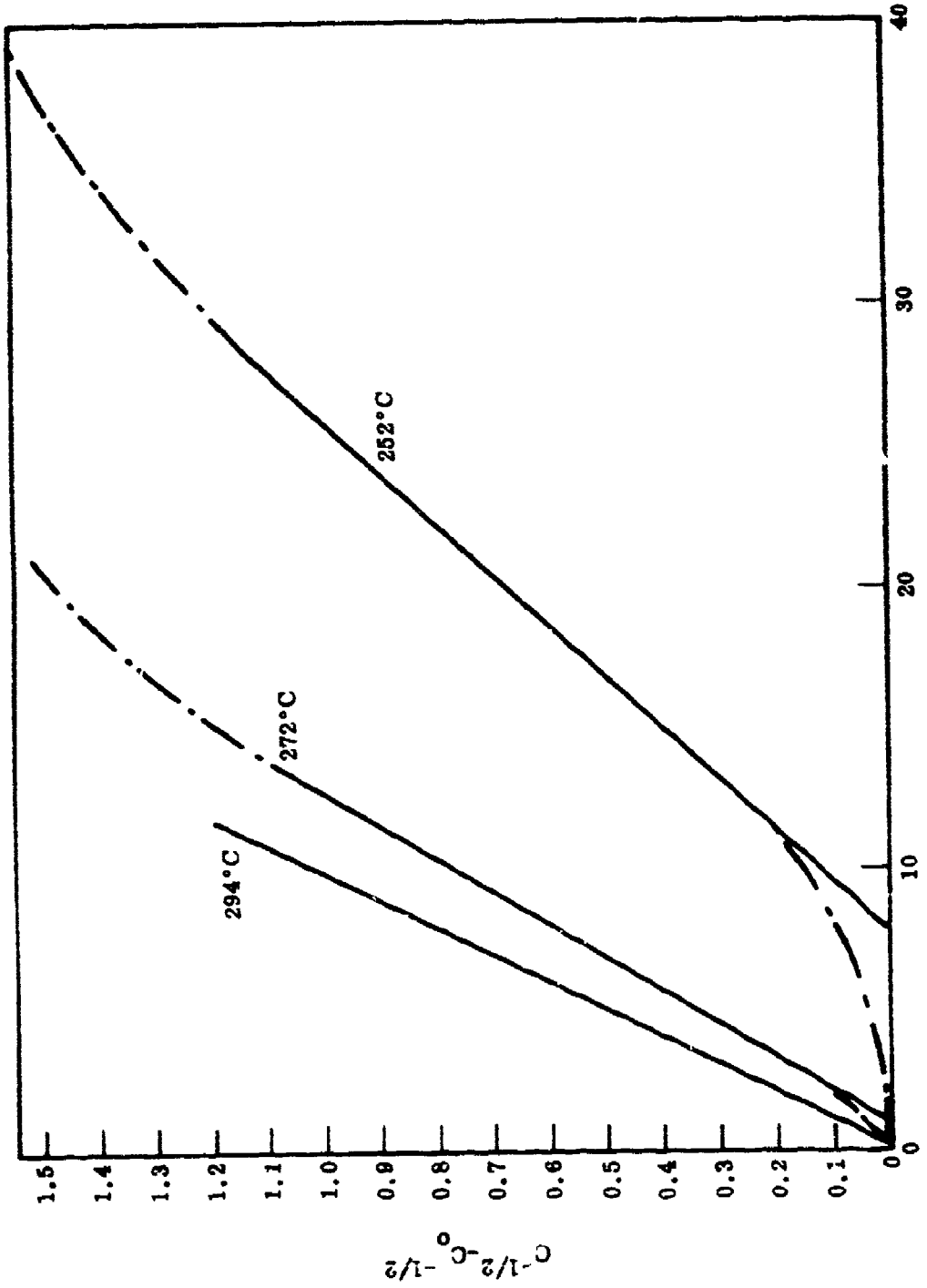

Fig. 6 Thermal Degradation of Polyvinyl Chloride Test of 3/2 Order Reaction Rate Law

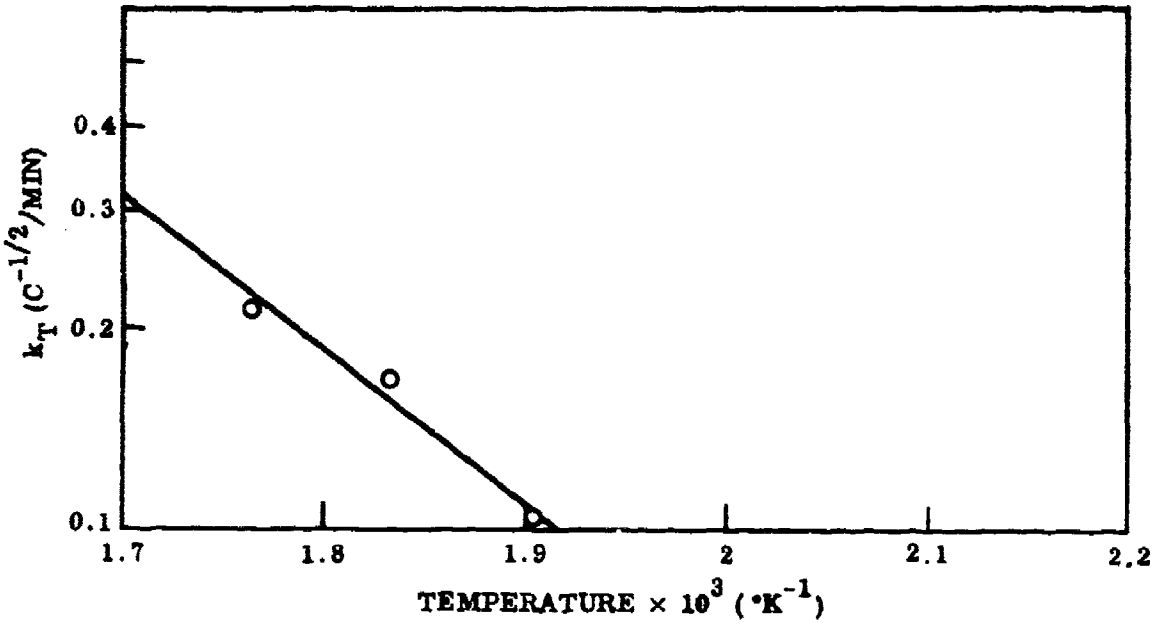

Fig. 7 Thermal Decomposition of Polyvinyl Chloride – Plot of Reaction Rate Constants

will require a two-zone decomposition model; moreover, this model is characterized by an exothermic low-temperature reaction followed by a high-temperature endothermic reaction. Such models, when programmed for computer analysis, tend to be costly in terms of machine time because of multiple zones. To simplify this analysis, this study will be confined to a two-component system – magnesium in strontium nitrate with weight fraction and particle size of the magnesium as variables.

2.4 EQUILIBRIUM CALCULATIONS FOR VARIOUS TRACER COMPOSITIONS

Several tracer compositions, both fuel-rich and stoichiometric (Table 3), were subjected to a computer study of the reaction products. The results are reported in terms of flame temperature, mole fraction in the gas phase, mol fraction in the solid phase, mole fraction in the solid phase based on the total composition, and the percentage of product moles to total moles of elements.

It will be noted from the results shown in Tables 4 through 9 that the product is chiefly composed of CO, H_2, gaseous Mg, N_2, and $SrCl_2$ and a solid phase which consists chiefly of MgO. The addition of PVC tends to shift the equilibrium from SrO to $SrCl_2$; in contrast, increasing the amount of oxidizer increases the water vapor at the expense of the hydrogen. In fuel-rich systems, unreacted magnesium and hydrogen are the chief reactive components if it can be assumed that the available oxidizer is effectively depleted within the bullet cavity. This finding would have the important simplifying implication (for fuel rich systems) that the critical parameters affecting the performance of the tracer munition are the kinetic and thermal transport processes occurring in the solid phase.

Table 3

PRODUCT DESCRIPTION FOR VARIOUS TRACER MIXTURES

Tracer Composition PVC/Mg/$Sr(NO_3)_2$ (Wt %)	Mixture Description	Flame Temperature (°K)	$\frac{\text{Moles Comb. Prod}}{\text{Moles of Elements}} \times 100$		
			3000	2500	2000
28.0 - 9.1 - 63.0	Stoichiometric	2960	43.66	42.01	41.92
19.8 - 12.7 - 67.5	Stoichiometric	3060	44.32	41.45	41.12
30.0 - 19.4 - 50.0	Fuel rich	2840	49.44	49.18	48.99
22.1 - 28.5 - 49.6	Fuel rich	2980	51.84	51.92	51.95
17.0 - 28.0 - 55.0	R-284	3070	50.07	50.02	50.04
17.0 - 33.0 - 50.0	Fuel rich	3070	53.24	53.37	53.40

Table 4

EQUILIBRIUM COMPOSITION OF REACTION PRODUCTS

TRACER COMPOSITION $\left(\text{PVC - Mg - Sr } (NO_3)_2\right)$ 28.0 - 9.1 - 63.0 wt %

Product	Mole Fraction					
	3000° K		2500° K		2000° K	
	Gas	Solid	Gas	Solid	Gas	Solid
CO	0.2616		0.2860		0.27 0	
CO_2	0.1043		0.1298		0.1417	
Cl	0.0012		0.0002		---	
HCl	0.0027		0.0023		0.0014	
$Mg Cl_2$	0.0005		0.0001		---	
H Mg O	0.0196		0.0014		---	
HO	0.0257		0.0039		0.0001	
H_2	0.0555		0.0727		0.0835	
H_2O	0.1595		0.2007		0.1943	
Mg	0.0609		0.0016		---	
NO	0.0060		0.0004		---	
N_2	0.1410		0.1633		0.1643	
O	0.0147		0.0002		---	
O_2	0.0170		0.0003		---	
Sr Cl_2	0.1198		0.1374		0.1386	
MgO		0.8053		0.8857		0.8891
(Fraction of Total Mole Product)		(0.089		(0.165)		(0.1677)
SrO		0.1947		0.1143		0.1109
(Fraction of Total Mole Product)		(0.0215)		(0.0213)		(0.0209)

Table 5

EQUILIBRIUM COMPOSITION OF REACTION PRODUCTS

TRACER COMPOSITION $\left(PVC - Mg - Sr(NO_3)_2\right)$ 19.8 - 12.7 - 67.5 wt %

Product	Mole Fraction					
	3000° K		2500° K		2000° K	
	Gas	Solid	Gas	Solid	Gas	Solid
CO	0.1953		0.1263		0.1088	
CO_2	0.1330		0.2540		0.2763	
Cl	0.0015		0.0003		---	
HCl	0.0025		0.0023		0.0015	
Mg Cl	0.0003		---		---	
H Mg O	0.0148		0.0007		---	
HO	0.0461		0.0087		0.003	
H_2	0.0317		0.0187		0.0205	
H_2O	0.1555		0.2290		0.2355	
Mg	0.0357		0.0003		---	
NO	0.0119		0.0021		---	
N_2	0.1896		0.2256		0.2294	
O	0.0251		0.0011		---	
O_2	0.0497		0.0053		---	
Sr Cl_2	0.1073		0.1256		0.1277	
MgO		0.7542		0.7862		0.7876
(Fraction of Total Mole Product)		(0.1995)		(0.2526)		(0.2554)
SrO		0.2458		0.2138		0.2124
(Fraction of Total Mole Product)		(0.065)		(0.06869)		(0.0685)

Table 6

EQUILIBRIUM COMPOSITION OF REACTION PRODUCTS

TRACER COMPOSITION $\left(PVC - Mg - Sr(NO_3)_2\right)$ 30.0 - 19.4 - 50 wt %

Product	Mole Fraction					
	3000° K		2500° K		2000° K	
	Gas	Solid	Gas	Solid	Gas	Solid
CO	0.2958		0.390		0.4017	
CO_2	0.0337		0.0029		---	
Cl	0.0044		0.0005		---	
H Cl	0.0131		0.0139		0.0029	
Mg Cl	0.0057		0.0040		0.0021	
$Mg Cl_2$	0.0022		0.0073		0.0144	
H Mg O	0.0270		0.0025		---	
HO	0.0141		0.0001		---	
H_2	0.1057		0.2430		0.2664	
H_2O	0.0869		0.0109		---	
Mg	0.2130		0.0957		0.0784	
NO	0.0014		---		---	
N_2	0.0953		0.1146		0.1171	
O	0.0042		---		---	
O_2	0.0014		---		---	
$Sr Cl_2$	0.0960		0.1146		0.1171	
MgO		1.0		1.0		1.0
(Fraction of Total Mole Product)		(0.0712)		(0.2175)		(0.2312)
SrO		0		0		0
(Fraction of Total Mole Product)		(0)		(0)		(0)

Table 7

EQUILIBRIUM COMPOSITION OF REACTION PRODUCTS

TRACER COMPOSITION $\left(\text{PVC - Mg - Sr } (NO_2)_3\right)$ 22.1 - 23.5 - 49.6 wt %

Product	Mole Fraction					
	3000° K		2500° K		2000° K	
	Gas	Solid	Gas	Solid	Gas	Solid
CO	0.2638		0.3237		0.3269	
CO_2	0.0219		0.0010		---	
Cl	0.0065		---		---	
H Cl	0.0015		0.0003		---	
Mg Cl	0.0009		0.0002		---	
H Mg O	0.0272		0.0023		---	
HO	0.0103		---		---	
H_2	0.1070		0.2110		0.2178	
H_2O	0.0640		0.0041		---	
Mg	0.2928		0.2217		0.2179	
NO	0.0011		---		---	
N_2	0.1116		0.1275		0.1283	
O	0.0031		---		---	
O_2	0.0007		---		---	
Sr Cl_2	0.0938		0.1080		0.1090	
MgO		0.9300		0.9557		0.9570
(Fraction of Total Mole Product)		(0.1908)		(0.2886)		(0.2938)
SrO		0.0701		0.0443		0.0430
(Fraction of Total Mole Product)		(0.01438)		(0.01337)		(0.0132)

Table 8

EQUILIBRIUM COMPOSITION OF REACTION PRODUCTS

TRACER COMPOSITION $\left(\text{PVC - Mg - Sr } (NO_3)_2\right)$ 17 - 28 - 55 wt %

Product	Mole Fraction					
	3000° K		2500° K		2000° K	
	Gas	Solid	Gas	Solid	Gas	Solid
CO	0.2631		0.3379		0.3434	
CO_2	0.0282		0.0019		---	
Cl	0.0006		---		---	
H Cl	0.0016		0.0004		---	
Mg Cl	0.0008		0.0002		---	
H Mg O	0.0260		0.9024		---	
HO	0.0128		---		---	
H_2	0.0980		0.2175		0.2287	
H_2O	0.0758		0.0073		---	
Mg	0.2265		0.1271		0.1190	
NO	0.0017		---		---	
N_2	0.1640		0.1922		0.1943	
O	0.0039		---		---	
O_2	0.0012		---		---	
$Sr Cl_2$	0.0956		0.1130		0.1145	
MgO		0.8732		0.9011		0.9028
(Fraction of Total Mole Product)		(0.3088)		(0.4011)		(0.4075)
SrO		0.1268		0.0989		0.0972
(Fraction of Total Mole Product)		(0.0448)		(0.04405)		(0.0439)

Table 9

EQUILIBRIUM COMPOSITION OF REACTION PRODUCTS

TRACER COMPOSITION $\left(PVC - Mg - Sr(NO_3)_2\right)$ 17 - 33 - 50 wt %

Product	Mole Fraction					
	3000° K		2500° K		2000° K	
	Gas	Solid	Gas	Solid	Gas	Solid
CO	0.2352		0.2785		0.2804	
CO_2	0.0165		0.0007		---	
Cl	0.0004		---		---	
H Cl	0.0013		0.0002		---	
Mg Cl	0.0009		0.0002		---	
H Mg O	0.0262		0.0022		---	
HO	0.0084		---		---	
H_2	0.0995		0.1823		0.1869	
H_2O	0.0505		0.0026		---	
Mg	0.3453		0.2969		0.2949	
NO	0.0010		---		---	
N_2	0.1290		0.1436		0.1442	
O	0.0026		---		---	
O_2	0.0005		---		---	
Sr Cl_2	0.0826		0.0928		0.0935	
MgO		0.8880		0.9120		0.9152
(Fraction of Total Mole Product)		(0.2620)		(0.3335)		(0.3369)
SrO		0.1120		0.0880		0.08684
(Fraction of Total Mole Product)		(0.0331)		(0.03219)		(0.0320)

2.5 THERMAL TRANSPORT PROPERTIES OF TRACER MIXTURES

The experimentally determined thermal transport properties are listed in Table 10 for mixtures of magnesium with strontium nitrate. These data are plotted in Figure 8. It will be observed that the conductivities of magnesium-rich mixtures are significantly below those of bulk magnesium (k = 0.38 cal/cm sec °K).

Table 10

THERMAL TRANSPORT PROPERTIES OF TRACER MIXTURES
Determined By Thermal Diffusivity Method (Ref. 3)

Mg (%)	$Sr(NO_3)_2$ (%)	Density (g/cm^3)	Thermal Diffusivity cm^2/sec	Heat Capacity (cal/°K g)	Thermal Conductivity (cal/cm-sec)°K
0	100	2.9	3×10^{-3}	0.18	1.57×10^{-3}
20	80	2.5	3.8×10^{-3}	0.193	1.83×10^{-3}
28.8	71.2	2.25	4.3×10^{-3}	0.196	1.9×10^{-3}
36.3	65.7	2.12	5.0×10^{-3}	0.203	2.15×10^{-3}
42.8	57.2	2.04	5.7×10^{-3}	0.207	2.41×10^{-3}
60	40	1.85	9.7×10^{-3}	0.218	3.9×10^{-3}
90	10	1.58	2.24×10^{-3}	0.236	8.35×10^{-3}
100	0	1.50	8.5×10^{-3}	0.244	3.11×10^{-2}
R-284		1.86	1.84×10^{-3}	0.210	0.72×10^{-3}

This behavior is typical of metal powders in which conductivity is controlled by surface and interstitial effects. Similarly, the conductivities of binary mixtures are significantly above that of R-284 which has 17-percent PVC. The findings of this study must therefore take into account the lower conductivities of actual tracer mixtures; otherwise, the model will not be affected.

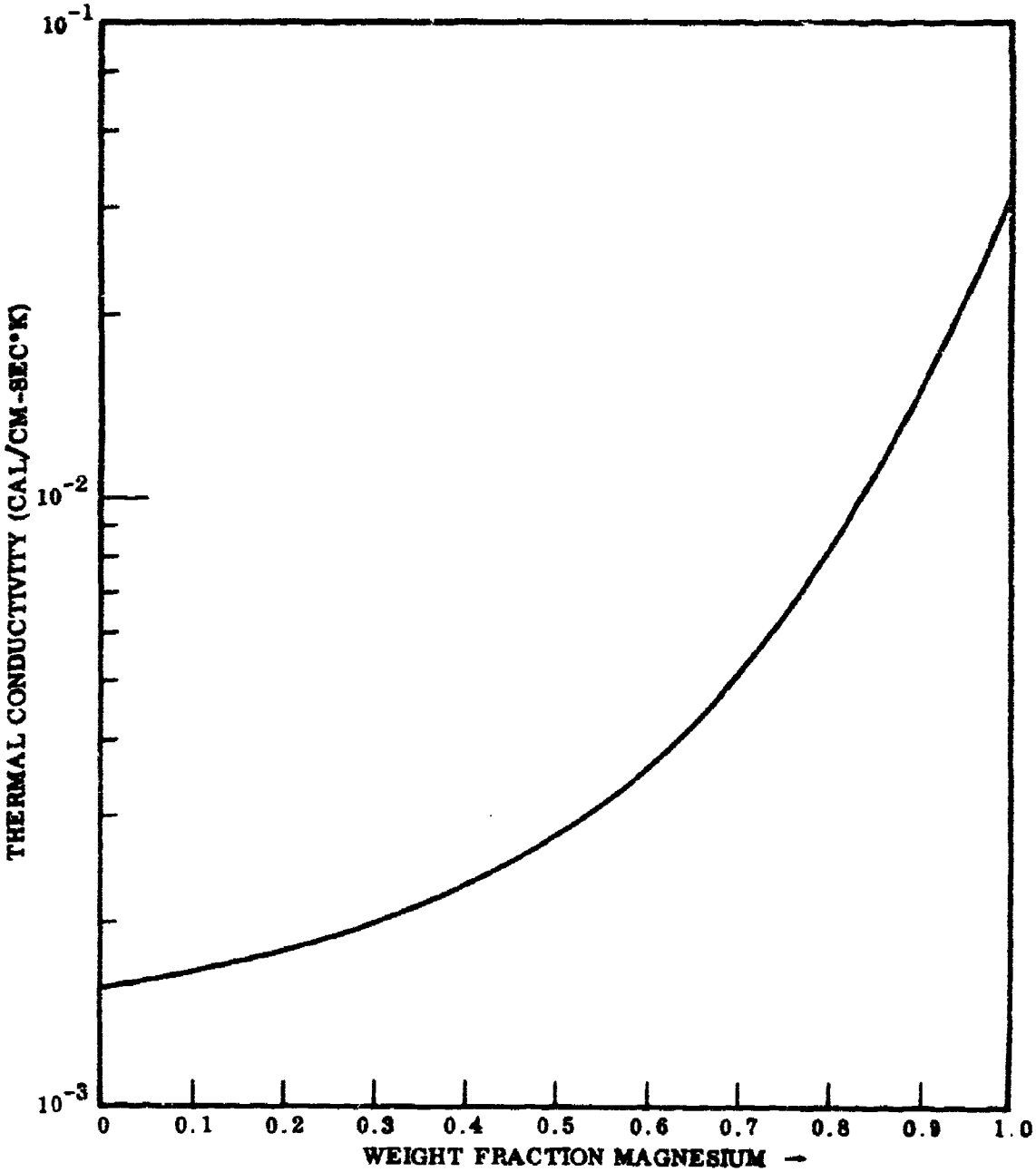

Fig. 8 Thermal Conductivity of Mg-$Sr(NO_3)_2$ Mixtures

Section 3
ANALYTICAL STUDY

3.1 SOLID-PHASE PROCESS

The mathematical representation of the thermal transport into the solid is pictured below.

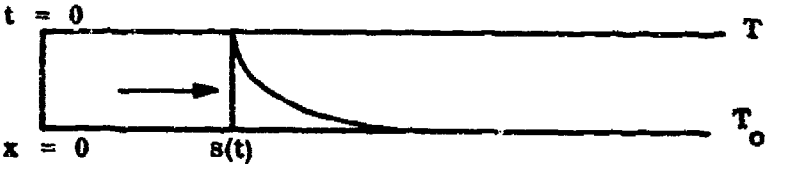

The location of the surface is denoted by s(t). It regresses at a constant speed $\frac{ds(t)}{dt}$, steady-state conditions being assumed.

The thermal transport process consists of the heat flux (H) into the surface and heat absorption by the thermal decomposition of $Sr(NO_3)_2$. The fusion of magnesium and the presence of the polyvinyl chloride are ignored. To aid in the visualization of the thermal processes, the individual steps are shown separately in Table 11. The thermal transport in the solid is described by

$$C_p \rho \frac{\partial T}{\partial t} = \kappa \frac{\partial^2 T}{\partial x^2} + \rho Q \frac{\partial F}{\partial t}, \quad x > 0, \; t > 0 \tag{11}$$

where

$$-\frac{\partial F}{\partial t} = F Z e^{-\frac{E}{RT}} \tag{12}$$

Table 11

SUMMARY OF THERMAL PROCESSES

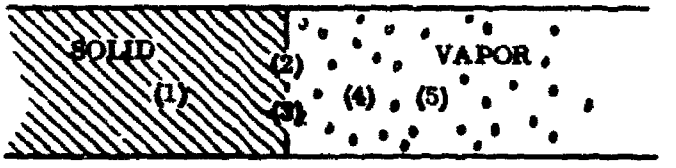

Zone 1

Decomposition of Polyvinylchloride

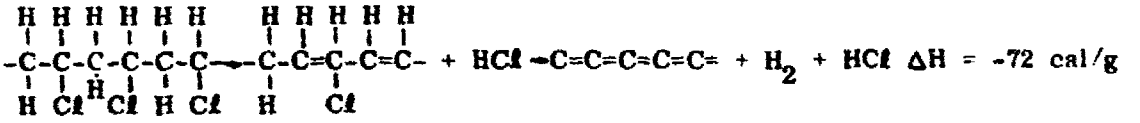

Zone 2

Decomposition of Strontium Nitrate

$$Sr(NO_3)_2 \longrightarrow SrO + 2\,NO_2 + 1/2\,O_2 \qquad \Delta H = +511\ cal/g$$

Zone 3

Melting of Magnesium

$$Mg_{(s)} \longrightarrow Mg_{(\ell)} \qquad \Delta H = +88.8\ cal/g$$

Zone 4

Vaporization of Magnesium

$$Mg_{(\ell)} \longrightarrow Mg_{(v)} \qquad \Delta H = +1300\ cal/g$$

Zone 5

Combustion of Magnesium Vapor

$$2\,Mg_{(v)} + NO_2 \longrightarrow 2\,MgO + N_2 \qquad \Delta H = -6000\ cal/g$$

$$2\,Mg_{(v)} + O_2 \longrightarrow 2\,MgO$$

Oxidizer rich composition absorbs $0.712 \times 511 + 0.288 \times 88.8 = 390$ cal/g

Stoichiometric composition absorbs $0.637 \times 511 + 0.363 \times 88.8 = 358$ cal/g

Fuel-rich composition absorbs $0.572 \times 511 + 0.428 \times 88.5 = 331$ cal/g

and

$$H + \kappa \frac{dT}{dx} = 0 \quad \text{at} \quad x = s(t) \tag{13}$$

The boundary conditions are

$$\left.\begin{aligned} T(s(t)) &= T_s \\ F(s(t)) &= 0 \end{aligned}\right\} \quad x = s(t) \tag{14}$$

Q is the heat of dissociation of strontium nitrate. The kinetic parameters Z and E are determined experimentally. The fraction F of undecomposed material has a fixed value at a given distance from the surface. The temperature gradient at the surface is determined by the heat flux H and by the thermal conductivity of the material [Eq. (13)]. These equations are solved numerically by a computer program that gives the regression rate when the heat flux is specified. This computer program is listed in the Appendix . A temperature profile is associated with each heat flux.

For a given heat flux, fuel-rich mixtures are expected to yield higher regression rates for two reasons: (1) the endothermic heat of decomposition varies linearly with oxidizer content; (2) a higher metal fraction brings about higher thermal conductivity. Experimental data on regression rates as reported in Table 12 are in agreement with this trend. The retarding effect of adding a binder (PVC) to the fuel-rich mixture is evident from the data on the R-284 mixture.

Table 12

EXPERIMENTALLY DETERMINED REGRESSION RATES
(furnished by Frankford Arsenal)

Description of Composition	Regression Rate (cm/sec) Ω = Spin Rate (rpm)	Burning Rate (cm/sec) at Ω = 40,000 rpm
Oxidizer Rich Composition 28.8% Mg 71.2% $Sr(NO_3)_2$	$0.15 + 4.66 \times 10^{-6} \Omega$	0.340
Stoichiometric Composition 36.3% Mg 63.7% $Sr(NO_3)_2$	$0.31 + 3.91 \times 10^{-6} \Omega$	0.466
Fuel-Rich Composition 42.8% Mg 57.2% $Sr(NO_3)_2$	$0.41 + 3.71 \times 10^{-6} \Omega$	0.550
R - 284 55% $Sr(NO_3)_2$ 28% Mg 17% PVC		0.272

3.2 GAS-PHASE REACTION

3.2.1 Introduction

The rate of energy release (heat flux) depends on the gas-phase reaction which, in turn, is governed by the particle size of the fuel and the gasification mechanism. The overall tracer burning rate depends on the energy partitioning between the energy deposited into the surface and the total energy output of the reaction. Some of the fuel-rich mixture will burn outside the bullet, but this is of no interest here. The energy partitions were not determined a priori, but were obtained from the experimentally determined regression rate.

Inspection of a motion picture (Ref. 1) of burning R-284 tracer mixture showed that magnesium particles are ejected from the pyrolyzing surface, and are then entrained in the stream of product gases. Some particles may undergo encapsulation by an oxide crust, followed by blow-out of the magnesium vapor (Fig. 1a), but it seems

that this mechanism may prevail only at the walls and other places that permit the physical entrapment of the particles. The reaction in the main gas stream appears to be one of a continuous boiloff from the exposed surface, causing each particle to trail a cloud of vapor or oxide (Fig. 1b).

3.2.2 Determination of the Magnesium Droplet Lifetime

The steady-state diffusion rate of the magnesium vapor from a droplet through a quasi-stationary layer of non-diffusing gas is given by

$$-\frac{dm}{dt} = \frac{D}{R\ T_s}\ 4\pi r\ (p_s - p_o) \tag{15}$$

where

$\frac{dm}{dt}$ = evaporation rate, mole/sec

r = radius of fuel droplet at time $t = \left(\frac{3\,m\,M}{4\,\pi\,\rho}\right)^{1/3}$

T_s = surface temperature of fuel droplet, 1363° K

p_s = partial pressure of magnesium at surface of droplet, 1 atm

p_o = partial pressure of magnesium in the gas stream, 0.12 atm (see Table 8)

ρ = density of magnesium, 1.74 g/cm^3

$$D = 0.0043\ \frac{T_a^{3/2}}{P\left(V_a^{1/3} + V_b^{1/3}\right)^2}\ \sqrt{\frac{1}{M_a} + \frac{1}{M_b}} \quad \text{(Ref. 12)} \tag{16}$$

where

M_a and M_b = molecular weights of air and magnesium

V_a and V_b = molecular volume for M_a and M_b

D = 358 cm^2/sec

Integrating the left side of Eq. (18) from m_o to 0 and the right side from $t = 0$ to $t = t_b$, the lifetime of the drop, one obtains

$$t_b = \frac{R T_s}{2 D} \frac{r_o^2 \rho}{M (p_s - p_o)} = 0.5 \times 10^{-3} \text{ sec} \qquad (17)$$

3.2.3 Calculation of Reaction Zone Thickness

During the time increment dt, the thickness of the gas layer freshly ejected from the solid surface is

$$(dx)_g = R T_a m_g y_n \rho_g v \, dt \qquad (18)$$

where

T_a = average temperature between the boiling magnesium (1363°K) and the flame temperature (3000°K, see Table 3), assumed to be 2000°K

m_g = moles of material in gas phase per gram of solid decomposed = 1.66×10^{-2}

y_n = mole fraction of nitric oxide and oxygen

ρ_g = density of gaseous mixture (including entrained solids)

v = regression rate (cm/sec)

At time t , the thickness of this oxidizing gas layer is reduced, by reaction with the magnesium, to

$$(dx)_g = \left(dx\right)_g^o \frac{m}{m_o} \tag{19}$$

m , the number of moles of magnesium in the drop at time t , is given by integration of Eq. (15), and when substituted into Eq. (19) gives the thickness of the combustion zone, x_c:

$$x_c = \frac{2ab^{5/2}}{5c} \tag{20}$$

where

$$a = \frac{R T_a m_g y_N \rho_g v}{m_o} \quad ; \quad b = m_o^{2/3} \quad ; \quad c = \frac{8\pi D}{3 R T_a} \left(\frac{3 M m_o}{4\pi\rho}\right)^{1/3}$$

Substituting, one obtains $x_c = 0.12$ cm.

Equation (20) permits the determination of the reaction zone thickness as function of particle size as shown in Figure 9. The finding that the reaction zone thickness is short compared with the depth of the bullet cavity agrees with published data (Ref. 13) which also indicate that for 80 mesh (175 μ) or smaller magnesium particles, the burning rate is not affected by particle size. We may conclude, therefore, that for mixtures which are close to stoichiometric proportions, the rate-determining processes occur in the solid phase.

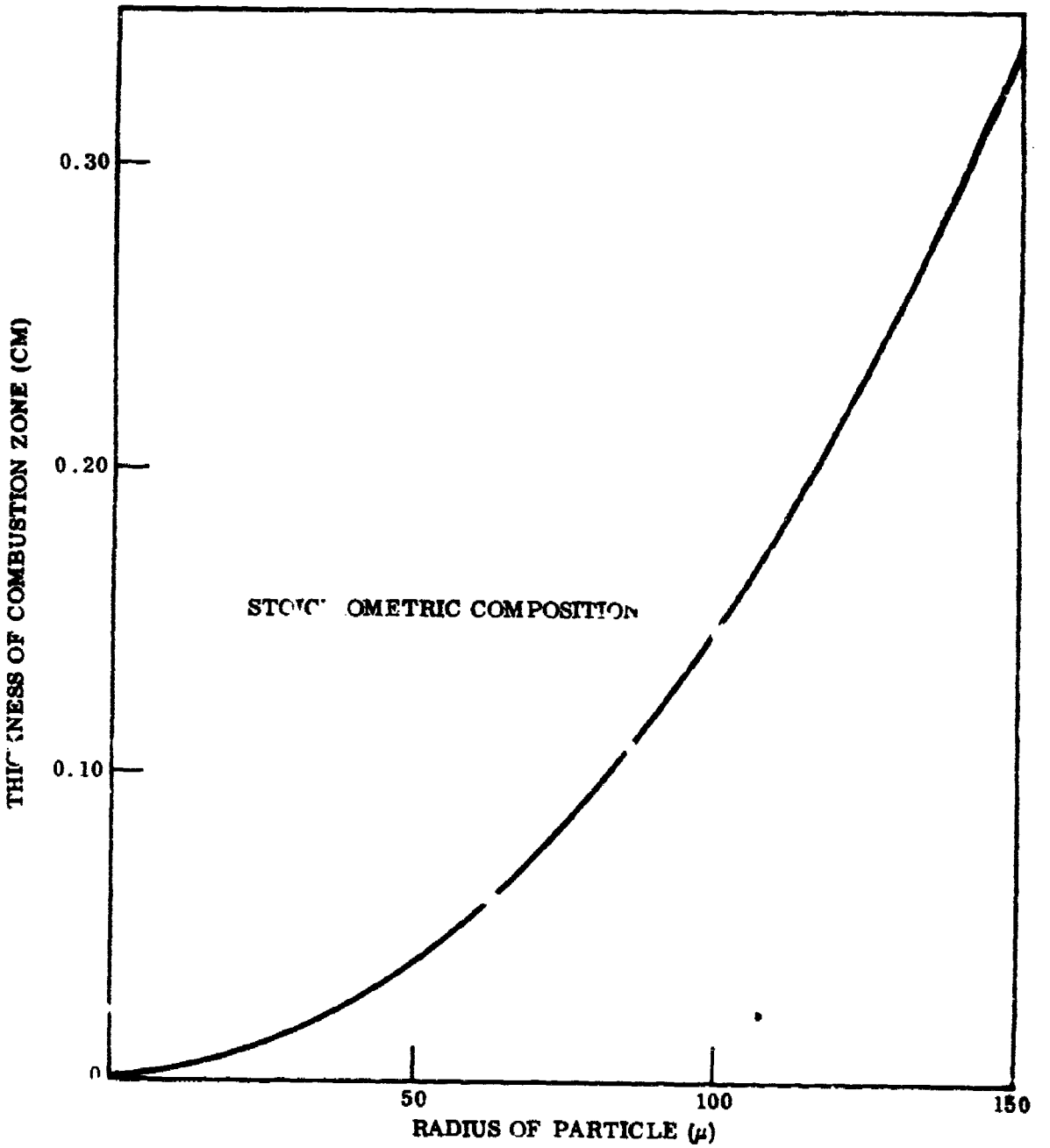

Fig. 9 Effect of Fuel Particle Size on Reaction Zone Thickness

Section 4
RESULTS

Figure 10 shows the temperature distribution in the solid phase as computed with the aid of the computer program listed in Appendix A. Figure 10 also shows that the surface temperature of the solid is above the melting point of magnesium because the model does not take into account the melting of the magnesium in the surface layer. If this refinement were to be incorporated, one would expect the surface temperature to be lower, somewhere between 1000 and 1300°K. Such a lowered surface temperature would bring out a steeper temperature profile, but any heat contributed by the decomposing PVC would tend to raise the temperature. Because of this fact, the simplification made in the model seems to be reasonable.

The particle size of the magnesium does not affect the temperature profile because the mixture was considered for computational purposes to be homogeneous. It will be noted that the particle size of the magnesium (0.012 cm) is of the same order as the solid reaction zone in the vicinity of the surface. Because the melting process is fast compared with the decomposition rate of the strontium nitrate, one may indeed expect the surface to consist of molten magnesium particles at a temperature which is somewhat below the boiling point (1363°K). This finding was confirmed by a motion picture study (Ref. 1).

Figure 11 shows the computed relationship between regression rate and heat flux into the solid. The model does not account for the spin effect on regression rate. Further, the effect of particle size (i.e., the thickness of the flame zone and hence the brightness of the luminous source) is contained within the heat flux and cannot be stated explicitly because the model does not account for the effect of the reaction zone

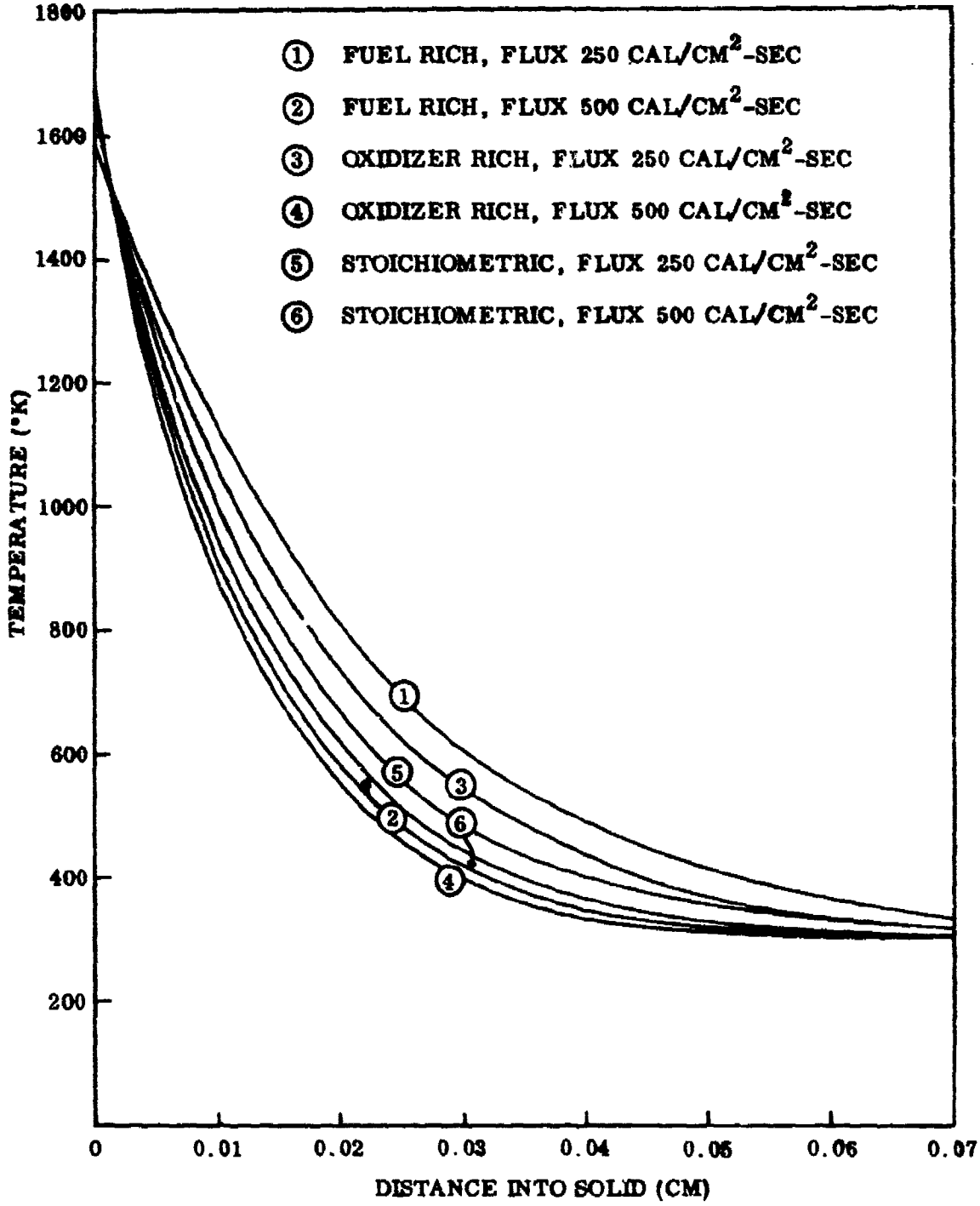

Fig. 10 Temperature Distribution in Solid

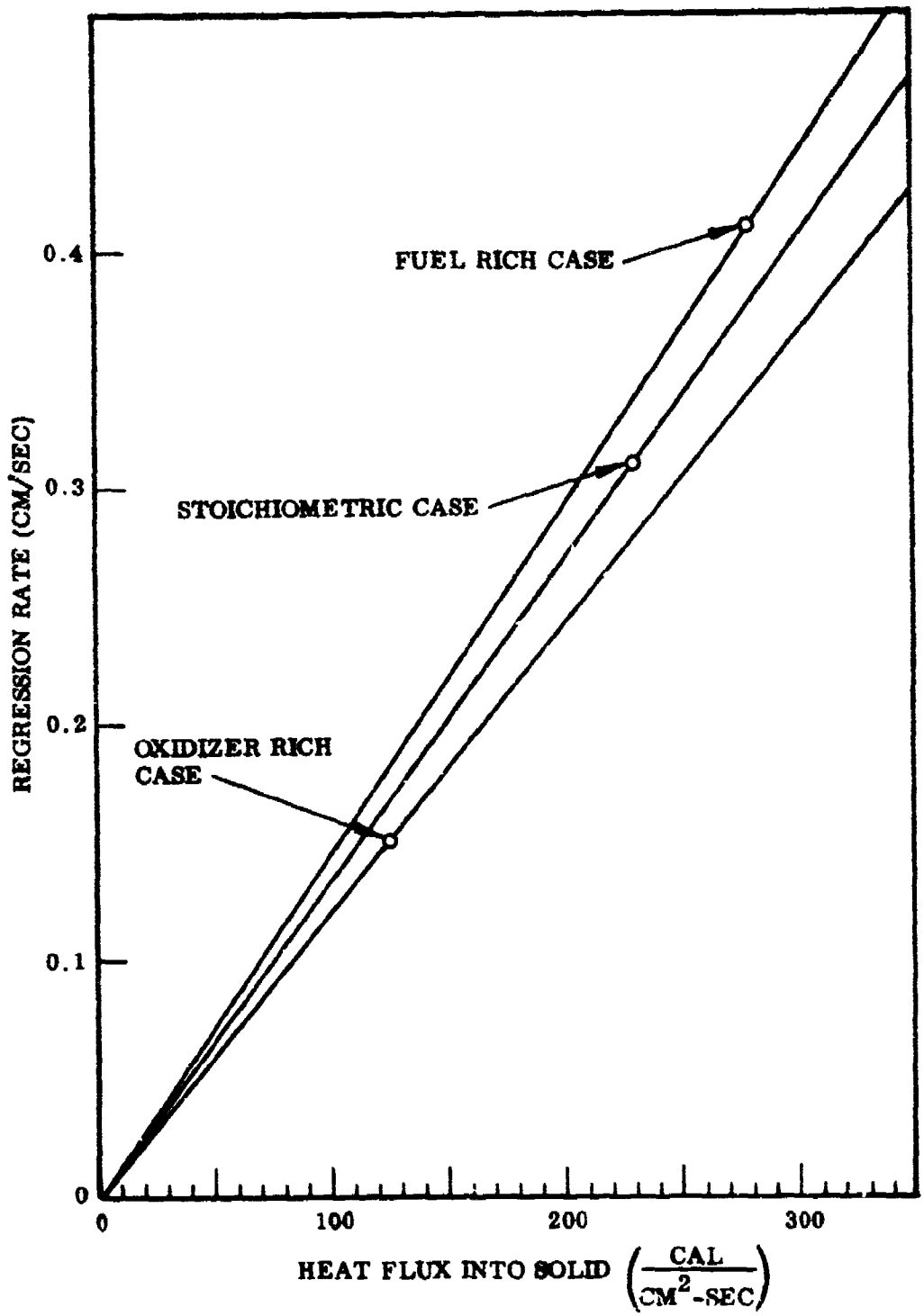

Fig. 11 Computed Reaction Rates as Function of Heat Flux. Data points were experimentally obtained at zero spin rate

thickness on the radiative heat transfer to the solid. We have shown (subsection 3.2), however, that the path length of the fuel particle is brief with respect to the depth of the tracer bullet cavity and, therefore, that for cases of particle sizes of less than 200μ and mixtures not very far removed from stoichiometric proportions, the findings of this study will be applicable.

Table 13 lists the heat fluxes and energy partitions for the cases for which experimental burning rates were available.

Table 13

CALCULATED HEAT FLUXES AND ENERGY PARTITIONS

Tracer Mixture	Regression Rate v, cm/sec	Heat Flux, Fig. 11 cal/cm^{2}sec	Energy Partition See Appendix B
Oxidizer Rich at $\Omega = 0$			
28.8% Mg, 71.2% $Sr(NO_3)_2$	0.15	125	27%
Stoichiometric at $\Omega = 0$			
36.3% Mg, 63.7% $Sr(NO_3)_2$	0.31	230	18.5%
Fuel Rich at $\Omega = 0$			
42.8% Mg, 57.2% $Sr(NO_3)_2$	0.41	280	20
R-284 at $\Omega = 40\,000$			
17% PVC, 28% Mg, 55% $Sr(NO_3)_2$	0.27	~220	-

If the model selected is valid in the presence of spin, the computed results shown in Figure 11 can also be used to study the effect of spin on the burning rate. We observe that heat flux into the solid increases with spin, whereas the energy partition is independent of spin. There are two reasons why the flux could increase with spin: (1) the centrifugal action may cause the ejected particles to be swept across the surface and so reduce the thickness of the boundary layer, or even erode the shape of the solid surface; and (2) the burning mechanism may change with spin as by the breakup of the reactive surface leading to the ejection of oxidizer and fuel aggregates into the gas stream. It may be helpful for the understanding of the burning mechanism to

have a motion picture study of the burning spinning tracer compositions, although the technical problems of resolving the surface phenomena will be formidable. A breakup of the solid would give rise to an extended reaction zone. It may be possible to assess this possibility by firing tracer bullets without spin (as from a smooth bore barrel using a sabot) or by investigating the plume generated in a laboratory bullet spinner. Such studies would also serve to confirm the findings of this study.

Section 5

RECOMMENDATIONS

The assumed decomposition model of the solid phase might be altered to allow for some oxidation reactions to occur in the solid as well as the ejection of some oxidizer aggregates from the surface prior to decomposition. This modification would no doubt be important in systems that contain a liquid phase in the reaction zone such as sodium nitrate (flare composition) or in which the gas phase reaction is of secondary importance (smoke generating munitions). A refinement of the computer program may be achieved by taking into account the melting of magnesium at the surface. In small-caliber ammunition, the deviations from the assumed one-dimensional geometry may become significant, and corrections for the heat losses to the container walls should be incorporated.

Application of the model to other types of munitions that may operate in an oxidizer-rich regime may require further study of the vaporization law used in this study. The presence of a diffusion barrier about the fuel particles (such as an oxide crust) will then become a significant factor in limiting the reaction rate.

The mechanism by which spin induces a change of burning rate may require further study. If the spin effect is due to a time-dependent phenomenon within the reaction chamber, the burning rate should not be assumed to be constant. Except for the experimental study required for an improved description of the spin effect, all other problems are amenable by an approach similar to the one chosen for this study.

A remaining problem area is the modeling of the energy partition. This task would require assigning the radiative, convective and conductive heat-transfer components so as to match experimentally determined energy partitions. The problem is made difficult by the complex radiation phenomena as well as by the possible deviation from steady-state conditions.

Section 6
SUMMARY AND CONCLUSIONS

The modeling of tracer reactions permits the determination of the parametric influence of composition on burning rate and of particle size on the reaction zone thickness. Neither a rigorous analysis of the effect of component and mixture characteristics on trace duration and trace visibility nor the mechanism of the effect of bullet spin on burning rate was included in this study. The tracer reaction appears to be completed within the bullet cavity so that the composition of the exit gases is accessible from equilibrium calculations. The influence of tracer compositions on the composition of exit gases was determined.

Thermal transport into solid tracer mixtures was found to be relatively insensitive to changes in composition. It was shown that all thermal processes that occur in the solid, such as dissociation and melting, occur with 200 μ from the surface, i.e., within a depth of no more than two fuel particles. The burning rate varies approximately linearly with heat flux, increasing with increased fraction of fuel. At the extremes in composition, this generalization is not expected to apply.

The model at present cannot predict the burning rate a priori without an experimental basis for the calculation of the energy partition which must account for the effect of spin on the reaction mechanism and for the relative importance of heat transfer modes within the bullet. At zero spin it was found that the burning rate is, for fuel-rich systems, insensitive to the fuel particle size, and that this finding is in agreement with previous studies. The methods employed in this study are expected to be of value in the study of other pyrotechnic devices such as fumer bullets, flares, and smoke canisters.

Section 7

REFERENCES

1. J. L. Eisel, "Burning R284 Pellet," AH 97-F1, 1974

2. Engineering Design Handbook, Part One, "Theory and Application AMCP 706-185, U.S. Army Material Command, April 1967, pp. 3 - 29

3. W. J. Panthen, R. J. Jenkins, C. P. Butler, and G. L. Abbott, "Flash Method of Determining Thermal Diffusivity, Heat Capacity, and Thermal Conductivity," J. Appl. Phys., Vol. 32, 1961, p. 1679

4. M. Centnerzwer and W. Piekielny, Bull. Int. Acad. Pol. Class. Sci. Math. Nat., 1933A, pp. 389–396

5. S. D. Shargorodskii and O. I. Shor, Ukrain. Khim. Zhur., Vol. 20, 1954, pp. 357-362

6. S. Gordon and C. Campbell, Anal. Chem., Vol. 27, 1955, pp.1102-1109

7. W. W. Wendlandt, The Texas Journal of Science, Vol. 10, 1958, pp. 392–398

8. E. S. Freeman J. Am. Chem. Soc., Vol. 79, 1957, pp. 838 - 842

9. M. Centnerzwer, Roczniki Chem., Vol. 18, 1938, pp.419-424

10. L. L. Lundberg, A. Jayaraman, C. L. Rohn, and R. G. Maines, Polymer Reprints, papers Presented at the Miami Beach Meeting, Vol. 8, April 1967, pp. 547-549

11. S. L. Madorsky, Thermal Degradation of Organic Polymers, New York, Interscience Publishers, 1964, pp. 160-172, see also R. R. Stromberg, S. Straus, and B. G. Achhammer, J. Polymer Sci., Vol. 35, 1959, p. 355

12. Gilliland, Ind. Eng. Chem., Vol. 26, 1934, p. 681

13. J. J. Caven and T. Stevenson, Pyrotechnics for Small Arms Ammunition, Frankford Arsenal Report R-1968, Jul 1970, p. 30

Appendix A
COMPUTER PROGRAM FOR THERMAL TRANSPORT IN THE SOLIDS

A.1 ORGANIZATION

After reading in the necessary input data, the program sets up the dimensionless variables and parameters, through the use of dimensionless groups.

Next, the input data and dimensionless groups are written out.

The calculation is then carried for successive time increments. At the end of each time increment, various dimensionless quantities are displayed for each distance increment.

A.2 INPUT

C	=	heat capacity
D	=	density
K	=	heat conductivity
Q	=	heat of endothermic reaction
Z	=	pre exponential factor
E	=	activation energy
HD	=	heat flux
TOD	=	initial temperature
DXD	=	distance increment
P	=	ratio of time increment to distance increment

EPS	=	small number indicating when decomposition is complete
NL	=	number of distance increments
MXT	=	maximum number of time increments allowed
NU	=	geometry factor (zero for one-dimension geometry)
ITERMX	=	maximum number of iterations allowed in the calculations

A.3 OUTPUT

For each time increments or a multiple number of time increments, the program prints out the following dimensionless quantities for each distance increment or for predetermined distance increments:

J	=	time index
TIME	=	dimensionless time
I	=	distance index
Dist	=	dimensionless distance
T	=	dimensionless temperature
F	=	fraction of nitrate undecomposed

When decomposition is complete in a distance increment, a message is printed out to this effect. The output table is then presented with that increment omitted.

Dimensionless time, distance and temperature can be converted to their dimensional counterparts, using multiplication factors given in the printout.

Regression rate can be obtained simply by dividing a burned-through distance by the corresponding time.

```
      REAL K
      DIMENSION T(200,4), F(200,4)
      DIMENSION ALPA(200), BETA(200), GAMA(200), PHI(200),A(200),PP(200)
      DIMENSION DELTA(200), G(200)
  100 FORMAT(8F10.4)
  102 FORMAT(8I10)
  200 FORMAT(1H1, 4HC = , E10.4, 5X, 4HD = , E13.4, 5X, 4HK = , E10.4,
     *5X, 4HQ = , E10.4, 5X, 4HZ = , E10.4, 5X, 4HE = , E10.4)
  202 FORMAT(1H0, 5HHD = , E10.4, 5X, 6HTOD = , E10.4, 5X, 6HDXD = ,
     *E10.4, 5X, 4HP = , E10.4, 5X, 6HEPS = , E10.4)
  204 FORMAT(1H0, 5HNL = , I4, 5X, 6HMXT = , I4, 5X, 5HNU = , I4, 5X,
     *9HITERMX = , I4)
  206 FORMAT(1H0, 9HTEMFCT = , F10.4, 5X, 9HTIMFCT = , E10.4, 5X,
     *9HDSTFCT = , E10.4, 5X, 4HB = , E10.4, 5X, 4HH = , E10.4)
  208 FORMAT(///1H0, 5X, 7HJ INDEX, 4X, 7HDL TIME, 5X, 7HI INDEX, 4X,
     *7HDL DIST, 7X, 7HDL TEMP, 7X, 10HDL UNREACT)
  210 FORMAT(1H0, 5X, I3, 5X, E10.4, 5X, I3, 5X, 3(E10.4,5X))
  212 FORMAT(1H0, 10X, 7HITER = , I3, 10X, 8HRATMX = , E10.4)
  214 FORMAT(///1H0,10X,21HNEW LAYER IS DEPLETED)
C     *****INPUT DATA*****
      READ(5,100) C, D, K, Q, Z, E
      READ(5,100) HD, TOD, DXD, P, EPS
      READ(5,102) NL, MXT, NU, ITERMX
      WRITE(6,200) C, D, K, Q, Z, E
      WRITE(6,202) HD, TOD, DXD, P, EPS
      WRITE(6,204) NL, MXT, NU, ITERMX
C     *****INITIALIZATION*****
      R = 2.0
      TEMFCT = R/E
      TIMFCT = R*Q*Z/C/E
      DSTFCT = SQRT(R*D*Q*Z/K/E)
      B = R*Q/C/E
      H = HD*SQRT(R/D/Q/Z/K/E)
      TO = TEMFCT*TOD
      DX = DSTFCT*DXD
      DT = P*DX**2
      PP1 = 1.0 + P
      PP1 = 1.0 - P
      P02 = P/2.0
      PDXH2 = 2.0*P*DX*H
      NLM1 = NL - 1
      WRITE(6,206) TEMFCT, TIMFCT, DSTFCT, B, H
      DO 300 I = 1, NL
      T(I,1) = TO
      F(I,1) = B
  300 CONTINUE
      TIME = 0.0
      IS = 1
C     ***** START DO LOOP FOR TIME INDEX J *****
      DO 332 J = 1, MXT
      JWRITE = 0
      IF(J .LE. 5 .OR. MOD(J,5) .EQ. 0) JWRITE = 1
      IF(JWRITE .EQ. 1) WRITE(6,208)
      TIME = TIME + DT
      N = MOD(J-1,4) + 1
      M = MOD(J,4) + 1
      NN = MOD(J+1,4) + 1
      MP = MOD(J+2,4) + 1
C     ***** FIRST STEP IN APPROXIMATE SOLUTION *****
      DO 304 I = IS, NLM1
      A(I) = FLOAT(NU)/2.0/FLOAT(I+1)
      PP(I) = EXP(-1.0/T(I,N))/9*DT
      IF(I .GT. IS) GO TO 308
      BETA(I) = PP1
      GAMA(I) = .P
      PHI(I) = PP1*T(I,N)+P*T(I+1,N)+PDXH2*P(I,N)*PP(I)
      DELTA(I) = GAMA(I)/BETA(I)
```

```
      G(I) = PHI(I)/BETA(I)
      GO TO 304
  308 ALFA(I) = PO2*(1.0-A(I))
      BETA(I) = -PP1
      GAMA(I) = PO2*(1.0+A(I))
      PHI(I) = -PO2*(1.0-A(I))*T(I-1,N)-PM1*T(I,N)-PO2*(1.0+A(I))*
     *T(I+1,N) + F(I,N)*PP(I)
      DELTA(I) = GAMA(I)/(BETA(I)-ALFA(I)*DELTA(I-1))
      G(I) = (PHI(I)-ALFA(I)*G(I-1))/(BETA(I)-ALFA(I)*DELTA(I-1))
  304 CONTINUE
      ALFA(NL) = PP1
      BETA(NL) = -P
      PHI(NL) = PM1*T(NL,N)+P*T(NL-1,N)-F(NL,N)*PP(NL)
      G(NL) = (PHI(NL)-ALFA(NL)*G(NL-1))/(BETA(NL)-ALFA(NL)*DELTA(NL-1))
C     ***** GETTING THE APPROXIMATE SOLUTION *****
      DO 306 I = NL, IS, -1
      IF(I .LT. NL) GO TO 310
      T(I,M) = G(I)
      IF(T(I,M) .LT. TO) T(I,M) = TO
      F(I,M) = F(I,N)*(1.0-PP(I))
      GO TO 306
  310 T(I,M) = G(I) - DELTA(I)*T(I+1,M)
      IF(T(I,M) .LT. TO) T(I,M) = TO
      F(I,M) = F(I,N)*(1.0-PP(I))
      IF(F(I,M) .LT. 0.0) F(I,M) = 0.0
  306 CONTINUE
      IF(JWRITE .NE. 1) GO TO 338
C     ***** WRITING OUT THE APPROXIMATE SOLUTION *****
      DO 312 I = 1, NL
      DIST = (I-1)*DX
      IF(I .LT. IS) WRITE(6,210) J, T    , I, DIST
      IF(I .GE. IS) WRITE(6,210) J,      , I, DIST, T(I,M), F(I,M)
  312 CONTINUE
  338 CONTINUE
C     ***** FIRST STEP IN IMPROVING THE    UTION *****
      DO 320 I = IS, NL
      T(I,NN) = T(I,M)
  320 CONTINUE
C     ***** BEGIN THE ITERATION *****
      ITER = 0
  328 ITER = ITER + 1
      NCAG = 0
      RATMX = 0.0
      DO 314 I = IS, NL
      PX = DT/B*EXP(-2.0/(T(I,NN)+T(I,N)))
      IF(I .GT. IS) GO TO 316
      T(I,MM) = 1.0/PP1*(PM1*T(I,N)+P*(T(I+1,NN)+T(I+1,N))+PDXH2
     *-(1.0-EXP(-PX))*F(I,N))
      GO TO 322
  316 IF(I .EQ. NL) GO TO 318
      T(I,MM) = 1.0/PP1*(PM1*T(I,N)+PO2*((1.0+A(I))*(T(I+1,NN)+T(I+1,N))
     *+(1.0-A(I))*(T(I-1,NN)+T(I-1,N))-(1.0-EXP(-PX))*F(I,N))
      GO TO 322
  318 T(I,MM) = 1.0/PP1*(PM1*T(I,N)+P*(T(I-1,NN)+T(I-1,N))*
     *(1.0-EXP(-PX))*F(I,N))
C     ***** 1 STATEMENT FOR TESTING *****
      T(I,MM) = TO
  322 RAT = (T(I,MM)-T(I,NN))/T(I,NN)
```

```
126*          ABSRAT = ABS(RAT)
127*          IF(ABSRAT .ST. EPS) NOAG = 1
128*          IF(ABSRAT .GT. RATMX) RATMX = ABSRAT
129*          PXX = DT/B*EXP(-2.0/(T(I,MM)+T(I,N)))
130*          F(I,NM) = F(I,N)*EXP(-PXX)
131*          IF(F(I,MM) .LT. 0.0) F(I,MM) = 0.0
132*      314 CONTINUE
133*      C       ***** THIS COMPLETES ONE ITERATION. *****
134*          ISD = 0
135*          JWRX = 0
136*          DO 326 I = IS, NL
137*          T(I,NM) = T(I,MM)
138*          RATE = F(I,MM)/B
139*          IF(RATE .LT. 1.0E-03) ISD = ISD + 1
140*          IF(RATE .LT. 1.0E-03) JWRX = 1
141*      326 CONTINUE
142*          IF(ITER .LE. ITERMX .AND. NOAG .EQ. 1) GO TO 328
143*          IF(JWRITE .NE. 1 .AND. JWRX .NE. 1) GO TO 340
144*          IF(JWRITE .EQ. 1 .AND. JWRX .NE. 1) GO TO 324
145*          WRITE(6,214)
146*      C       ***** WRITING OUT THE IMPROVED SOLUTION *****
147*      324 WRITE(6,212) ITER, RATMX
148*          DO 330 I = 1, NL
149*          DIST = (I-1)*DX
150*          IF(I .LT. IS) GO TO 334
151*          WRITE(6,210) J, TIME, I, DIST, T(I,MM), F(I,M)
152*          GO TO 330
153*      334 WRITE(6,210) J, TIME, I, DIST
154*      330 CONTINUE
155*      C       ***** START THE NEXT TIME CYCLE *****
156*      340 IS = IS + ISD
157*          DO 342 I = 1, NL
158*          T(I,M) = T(I,MM)
159*          F(I,M) = F(I,MM)
160*      342 CONTINUE
161*      328 CONTINUE
162*          END
```

Appendix B
CALCULATION OF ENERGY PARTITION

Heat Generation, Stoichiometric Case

$$5\ Mg + Sr\ (NO_3)_2 \rightarrow 5\ MgO + SrO + N_2$$

$$\Delta H_R = 1880\ cal/g$$

Rate of Heat Generation, Case of Zero Spin (see Tables 12 and 13)

$$\Delta H_R \times \rho \times v = 1235\ \frac{cal}{sec\ cm^2}$$

Heat Flux into Solid (see Fig. 11)

$$H = 230\ \frac{cal}{sec\ cm^2}$$

Energy Partition: 230/1235 = 18.5%

Similarly, for Spin Rate of 40,000 rpm

$$H = 340$$

Energy Partition: $\frac{340}{1855} = 18.5\%$

It must be remembered that Fig. 11 was not based on a model which included a spin effect. It is possible that a refined model would not yield the same conclusion, i.e., that the energy partition is independent of spin.